

# Nanoindentation of LaCrO<sub>3</sub> thin films

ANTHONY MARIO CORATOLO, NINA ORLOVSKAYA\*

*Department of Materials Science and Engineering, Drexel University, 3141 Chestnut Str., Philadelphia, PA 19104*

*E-mail: orlovsk@drexel.edu*

M. LUGOVY, V. SLYUNYAYEV

*Institute for Problems of Materials Science, 3 Kzhizhanovskii Str., 03142, Kiev, Ukraine*

S. DUB

*Institute of Superhard Materials, 2 Avtozavodskaya Str., 04074, Kiev, Ukraine*

CHRISTOPHER JOHNSON, RANDALL GEMMEN

*National Energy Technology Laboratory, Department of Energy, 3610 Collins Ferry Road, Morgantown, WV, 26507*

**Published online:** 17 January 2006

Nanoindentation of LaCrO<sub>3</sub> thin films deposited by radio-frequency magnetron sputtering onto stainless steel substrates was performed using an XP Nanoindenter. The “as-deposited” film was amorphous but transformed to an orthorhombic LaCrO<sub>3</sub> perovskite structure after annealing at 1073 K for 1 h. The film thickness in the “as-deposited” state was 800 nm. Single loading/unloadings were performed in the displacement control mode on the crystalline film using different maximum displacements (50, 200, 400, and 800 nm). Therefore, the integral response of the film–substrate system was probed at different distances from the substrate. Nanoindentation experiments on LaCrO<sub>3</sub> perovskite films revealed sharp “pop-in” events at certain loads. Such “pop-ins” are most likely caused by the orthorhombic-to-rhombohedral phase transition which is known to occur in a LaCrO<sub>3</sub> perovskite structure under pressure. However, such discontinuities have never been observed upon indentation of the amorphous “as-deposited” La-Cr-O thin films, and the pressure found to be typical of this transition in the LaCrO<sub>3</sub> thin films is higher than previous bulk LaCrO<sub>3</sub> sample studies. Mechanical characteristics of the films, such as hardness and Young’s modulus, were also measured.  
© 2006 Springer Science + Business Media, Inc.

## 1. Introduction

In the last ten years nanoindentation has become a very important method of characterizing both mechanical properties and deformation behavior of materials under contact loading [1–3]. It can also provide insight into pressure-induced structural changes such as dislocation nucleation, amorphization, and phase transitions developing in different materials upon their indentation [4–6]. Nanoindentation is especially effective and convenient for the evaluation of mechanical behavior of thin films, where frequently other methods are not available. Such properties as Young’s modulus and hardness can easily be measured for novel thin film materials, even when their mechanical characteristics are not known in advance.

Despite the ease with which nanoindentation can be applied to the study of thin film properties, care must be taken in the analysis of the indentation response, since there are a number of film and indenter parameters that will affect the films response to contact loading. The nanoindentation response is sensitive to surface roughness, residual surface stresses, elastic anisotropy, texture, film thicknesses, and substrate characteristics. The indenter tip geometry can also have a significant effect because of the small penetration depth, which is limited by the film thickness. Nanoindentation is also strongly affected by different deformation processes occurring under the indenter during loading/unloading of the film.

\*Author to whom all correspondence should be addressed.

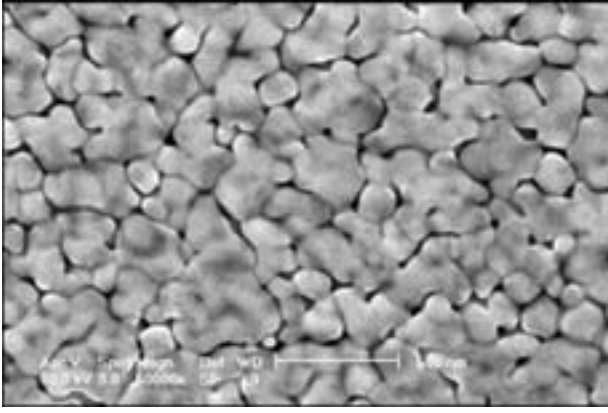


Figure 1 Microstructure of a LaCrO<sub>3</sub> perovskite thin film.

Magnetron sputter deposited La-Cr-O thin films are amorphous when deposited on an ambient temperature substrate. An amorphous-to-crystalline transformation starts upon annealing at high temperatures in air. This transition occurs in the two steps, viz. first the material is transformed to a monoclinic LaCrO<sub>4</sub> monazite phase at 803 K and after annealing at 1073 K, a further transformation to an orthorhombic LaCrO<sub>3</sub> perovskite structure takes place [7]. During the phase transition from LaCrO<sub>4</sub> to LaCrO<sub>3</sub>, oxygen is released from the lattice and a loss of oxygen leads to about a 30% decrease in its molecular volume, which corresponds to about a 10% decrease in LaCrO<sub>3</sub> grain sizes. Such a volume decrease gives rise to the structure containing self-organized dendrites with a substantial degree of porosity (Fig. 1).

In bulk samples, LaCrO<sub>3</sub> has an orthorhombic structure with the lattice constants  $\sim\sqrt{2}ap \times \sim\sqrt{2}ap \times 2ap$ , where  $ap$  is the lattice constant of a pseudo-cubic perovskite structure [8] at room temperature and under atmospheric pressure. It exhibits a first-order orthorhombic (space group  $Pbnm$ , #62) to rhombohedral (space group  $R\bar{3}c$ , #167) phase transition in response to pressure and temperature [9, 10]. Significant volume compression due to the shrinkage of CrO<sub>6</sub> octahedra was observed in the case of the LaCrO<sub>3</sub> orthorhombic-to-rhombohedral phase transition at about 533 K [11], with a linear thermal expansion coefficient changing from  $7.73 \times 10^{-6} \text{ K}^{-1}$  at 480 K to  $-17.64 \times 10^{-6} \text{ K}^{-1}$  at 542 K [12]. A pressure-induced LaCrO<sub>3</sub> phase transition has also been reported [9, 11]. The orthorhombic-to-rhombohedral transition in LaCrO<sub>3</sub> occurred at a pressure up to 5.4 GPa. The crystal system of LaCrO<sub>3</sub> was shown to be orthorhombic at room temperature and atmospheric pressure but it becomes rhombohedral at a pressure of 5.4 GPa. It was also shown that at pressures within 1.1 and 5.1 GPa, a mixture of orthorhombic and rhombohedral phases existed. From simple considerations of enthalpy and molar volume variations at a phase transition [13], it was concluded that the rhombohedral phase could be thermodynamically stable under a pressure as low as 0.53 GPa at room temperature.

Findings on the indentation response of LaCrO<sub>3</sub>-based perovskite ceramics have not been reported to date, al-

though it is a very valuable material widely used as an interconnect in SOFCs [14], as an anticorrosive coating of metallic SOFC interconnects [15], or as heat exchangers [16]. Its applicability to the SOFC applications is primarily due to its relatively good electronic conductivity [17], and its high phase stability in both oxygen and hydrogen environments. Knowledge of the LaCrO<sub>3</sub> deformation behavior under concentrated loading, and the accurate measurement of the mechanical properties are of great importance. For instance, the elastic properties can be used to determine the interface fracture toughness of the film/substrate pairing [18]. In this paper the results of nanoindentation of RF magnetron-sputtered LaCrO<sub>3</sub> perovskite films deposited onto stainless steel substrates as a method of determining their deformation behavior under contact loading are presented as well as the measured values of hardness and Young's modulus.

## 2. Materials and experiments

Thin films were deposited by RF magnetron sputtering onto Cr-containing stainless steel (SS) substrates. High-chromium ferritic Fe-25Cr steel coupons (SS 446) with the following chemical composition: Fe (74 wt%), Cr (23 wt%), Mn (1.5 wt%), Ni (0.3 wt%), Si (1.0 wt%), C (0.2 wt%) were used as a substrate material. Stainless steel substrates (10 × 10 × 5 mm) were polished with a diamond spray to a mirror surface. To determine Young's modulus and hardness of the substrate, nanoindentation was performed and these parameters were measured to be 220.2 GPa and 2.5 GPa, respectively. Light green La-Cr-O films were deposited as a result of 8-h magnetron sputtering. An "as deposited" film thickness, measured by phase shift technology using an interferometric surface profiler, was 800 nm. EDS analysis of the "as-deposited" film composition gave a La/Cr ratio of 56.54/43.46 at%. The "as-deposited" film and samples annealed in air at 1073 K for 1 h were analyzed by XRD. The "as-deposited" film was found to be X-ray amorphous [19], and the orthorhombic LaCrO<sub>3</sub> structure was determined after annealing of the film. The crystalline LaCrO<sub>3</sub> films were used in nanoindentation experiments.

Nanoindentation tests of LaCrO<sub>3</sub> perovskite thin films were performed using an XP nanoindenter (MTS Systems) at room temperature. In the tests the Berkovich diamond indenter was used. To account for indenter tip irregularities, the projected contact area estimated by evaluating of the indenter shape function was used in calculations,

$$A(h_c) = 24.4648h_c^2 + 5000h_c + 1123.26h_c^{1/2} + 312.683h_c^{1/4} + 165.257h_c^{1/8}, \quad (1)$$

here  $h_c$  is the contact depth [1, 20]. The area factors were fitted to the experimental data obtained with the Berkovich indenter. Nanoindentation tests were performed in the displacement control mode with a maximum 800-nm displacement allowed. At least 10 indents were made for

each test with significant distances between them. Loading and unloading rates were the same in each cycle, however, from cycle to cycle they varied from 0.022 to 0.42 mN/s.

The average contact pressure (ACP), was calculated from nanoindentation data by a procedure described in [21, 22]. The average contact pressure  $\sigma_i$  is defined as

$$\sigma_i = \frac{P_i}{A_i}, \quad (2)$$

where  $P_i$  is the applied load and  $A_i$  is the projected contact area (current contact area). Contact area was found using accumulated load-displacement data. The elastic deflection at maximum load  $(h_s)_{\max}$  was calculated from [1]:

$$(h_s)_{\max} = \varepsilon \frac{P_{\max}}{S}, \quad (3)$$

where  $\varepsilon$  is the geometrical constant equal to 0.72,  $P_{\max}$  is the maximum measured load, and  $S$  is the slope of the unloading portion of the load-displacement diagram at the beginning of unloading. Next, the current elastic deflection  $(h_s)_i$  was determined from [21, 22]

$$(h_s)_i = (h_s)_{\max} \sqrt{\frac{P_i}{P_{\max}}} \quad (4)$$

This relationship is obtained from contact mechanics [3]. Finally, the depth of the material in contact with the indenter  $(h_c)_i$  was found as

$$(h_c)_i = h_i - (h_s)_i, \quad (5)$$

where  $h_i$  is the indenter displacement at the  $i$ th data point measured experimentally. Now, the current contact area was calculated from Equation 1 substituting  $(h_c)_i$  for  $h_c$ . Thus, using applied load values obtained from measured load-displacement data and corresponding calculated contact area values, one can directly obtain ACP values for all the data points from Equation 2.

### 3. Results and discussion

Nanoindentation is known to be an ideal instrument for studying mechanical properties of thin films. Contact loading also provides information on structural changes

(e.g., ‘‘pop-in’’ and/or ‘‘pop-out’’ events) that produce sudden displacements with little or no force change upon loading and unloading [1, 4, 23]. Indentation responses along with the plastic/elastic behavior of LaCrO<sub>3</sub> perovskite thin films were investigated and mixed plastic and elastic responses were observed upon deformation of the film.

The elastic response can adequately be characterized by the residual displacement (corresponding to unloading)—maximum displacement ratio [24]. This parameter, independent of a displacement due to the self-similarity of the indenter geometry, is easily determined from experimental data. Natural variation ranges for this parameter are  $0 \leq h_f/h_{\max} \leq 1$ . The lower limit corresponds to purely elastic strain and, thus, to the complete recovery of the material upon unloading. The upper limit characterizes the rigid-plastic material with no elastic recovery.

An alternative parameter, characterizing elastic recovery upon indentation, is the ratio of the work spent for plastic strain  $W_p$  to the total work  $W_t$  performed upon loading. The total work required for indentation of the material to the maximum load  $P_{\max}$ , i.e., the work of external force for producing an indent corresponding to  $P_{\max}$ , is  $W_t \equiv \int_0^{h_{\max}} P dh$  (the integral is taken over the loading portion of the indentation diagram). The work spent for plastic strain equals  $W_p = W_t - W_e$ , where  $W_e \equiv \int_{h_f}^{h_{\max}} P dh$  is the energy of elastic strains released upon unloading (the integral is taken over the unloading portion of the indentation diagram). The ranges for the parameter are  $0 \leq W_p/W_t \leq 1$ . If  $W_p/W_t = 0$ , purely elastic strain and, consequently, the complete recovery of the material surface after complete unloading is expected. The case of  $W_p/W_t = 1$  corresponds to the rigid-plastic material, which exhibits no elastic recovery.

Proceeding from the notion that the loading and unloading portions of the indentation diagram can be represented by  $P = Ch^2$  and  $P = B(h - h_f)^2$  curves ( $C$  is the indentation curvature), one might reason [25, 26] that  $h_f/h_{\max} = W_p/W_t$ , which points to the equivalence of energy and displacement-based approaches. However, it was demonstrated [27] that the equality  $h_f/h_{\max} = W_p/W_t$  is a good approximation only in the particular case, when  $h_f/h_{\max}$  is close to unity. In the general case this equality is not observed.

The  $h_f/h_{\max}$  and  $W_p/W_t$  values for LaCrO<sub>3</sub> thin films calculated at different displacements/loads are summarized in Table I. As one can see the  $h_f/h_{\max}$  and  $W_p/W_t$

TABLE I Plasticity of LaCrO<sub>3</sub> perovskite thin films after nanoindentation results

Film composition	Maximum displacement (nm)	Load (mN)	With ‘pop-in’		Without ‘pop-in’	
			$h_f/h_{\max}$	$W_p/W_t$	$h_f/h_{\max}$	$W_p/W_t$
LaCrO <sub>3</sub>	50	0.98	–	–	0.64	0.59
LaCrO <sub>3</sub>	200	8.20	0.72	0.76	0.71	0.85
LaCrO <sub>3</sub>	400	20.70	0.83	0.74	0.79	0.75
LaCrO <sub>3</sub>	800	55.30	0.88	0.90	0.89	0.93

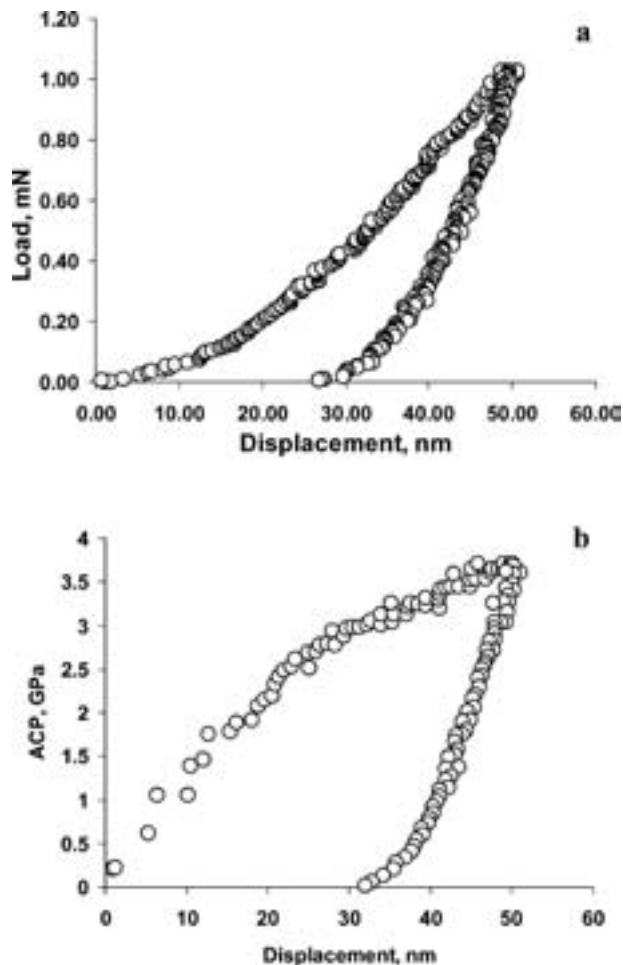


Figure 2 Load vs. displacement (a) and ACP vs displacement (b) diagrams at a preset maximum displacement of 50 nm.

parameters are not equal, i.e.,  $h_f/h_{\max} > W_p/W_t$  in case of both 50 and 400 nm displacement (with “pop-in” and without it). However, at 200 and 800 nm displacements, the inverse inequality  $h_f/h_{\max} < W_p/W_t$  is observed in both cases (with “pop-in” and without it). With an increase in displacements, the  $h_f/h_{\max}$  and  $W_p/W_t$  parameters show a general increase that can be explained by the presence of a more plastic substrate. At a given displacement, the  $h_f/h_{\max}$  ratios for the cases with “pop-in” and without it are slightly different. The same relationship is also true for the  $W_p/W_t$  parameters, which points to a weak influence of “pop-in” associated processes on the film plasticity.

The effect of a substrate on the indentation diagrams can be neglected for the case of a displacement not exceeding a 10% film thickness [28]. But for the thicknesses of thin films used in the present study, the substrate effect on the indentation diagram (especially at large displacements) cannot be ignored. The sole exception is the data obtained at a 50 nm displacement where the materials properties can be assigned to the  $\text{LaCrO}_3$  material.

The response of a film indented at a displacement less than a 10% film thickness is shown in Fig. 2a. The hardness and Young’s modulus of the film calculated accord-

ing to the Oliver and Pharr technique [1] were 3.1 GPa and 162 GPa, respectively. An ACP exhibited a maximum value of 3.8 GPa at maximum loads (Fig. 2b). No “pop-in” events were observed upon nanoindentation at such small loads.

As the displacement/contact area increased with an increase in indentation loads, the two types of deformation curves could be seen (Fig. 3a and b). For the majority of indentation tests, no significant discontinuities were observed both upon loading and unloading of the film (Fig. 3a). An ACP first increased up to 6 GPa with a further decrease down to 4.7 GPa at maximum loads (Fig. 3c). Elastic loading of the specimen surface is affected by blunting of the indenter tip. At a displacement of about 60 nm, a constrained plastic strain zone crops out at the specimen surface and plastic flow starts in the contact area. Then ACP in the indent starts decreasing slowly, which is the effect of a pliant substrate. Plastic flow usually develops at a displacement of about 20 nm [29], however in our case it happens at a 60 nm displacement, probably because of significant blunting of the indenter tip. In some cases pronounced discontinuity (“pop-in”) was observed upon loading of the film (Fig. 3b). Since upon unloading, “pop-out” was absent, the event was irreversible. Plastic flow starts at a 50-nm displacement (change in the slope of the curve). But an increase in pressure in the contact area continues down to a displacement of about 170 nm. A calculated ACP increased upon loading reaching a maximum value of 8 GPa at the beginning of “pop-in”, which was only 5 GPa at the end of “pop-in” (Fig. 3d). During such a “pop-in” a drastic volume decrease should occur.

Indentation to maximum displacements (400 and 800 nm) resulted in the two characteristic load–displacement diagrams. In both cases, “pop-in”- free (Figs 4a and 5a) and “pop-in” (Figs 4b and 5b) diagrams are also observed. At a 400 nm displacement and in the absence of “pop-in”, an ACP first increases up to 5.9 GPa, then falls down to 3.9 GPa (Fig. 4c). In the presence of “pop-in”, an ACP grows up to 6.8 GPa, then falls down to 3.7 GPa (Fig. 4d). At an 800 nm displacement and in the absence of “pop-in”, an ACP first grows up to 5.2 GPa, then decreases down to 2.8 GPa (Fig. 5c). In the presence of “pop-in”, an ACP increases up to 7.1 GPa followed by its decrease down to 2.6 GPa (Fig. 5d). Therefore in all cases “pop-in” events occur when the contact pressure is higher than 6.86 GPa.

Hardness and Young’s modulus values as a function of the displacement are shown in Fig. 6a and b, respectively. Both hardness and Young’s modulus values, corresponding to  $>50$  nm displacements, can be considered only as a qualitative integral characteristic of the material accounting for the effect of the film and substrate and only the integral reaction of the film–substrate system is obtained. Hardness and Young’s modulus corresponding to the properties of the film material should be measured only when a displacement is equal to 50 nm. When a displacement is equal to the film thickness, hardness and Young’s modulus corresponding to the substrate are prac-

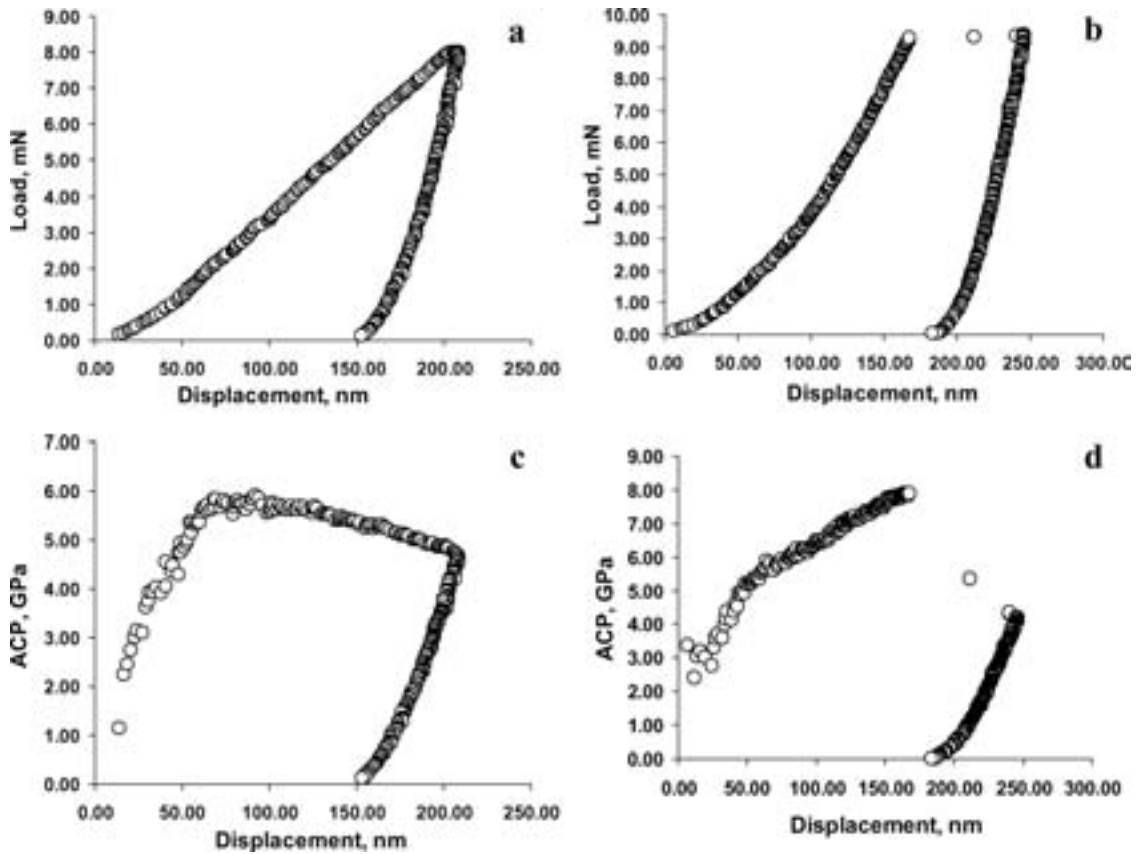


Figure 3 Load vs displacement (a—without “pop-in”, b—with “pop-in”) and ACP vs displacement (c—without “pop-in”, d—with “pop-in”) diagrams at a preset maximum displacement of 200 nm.

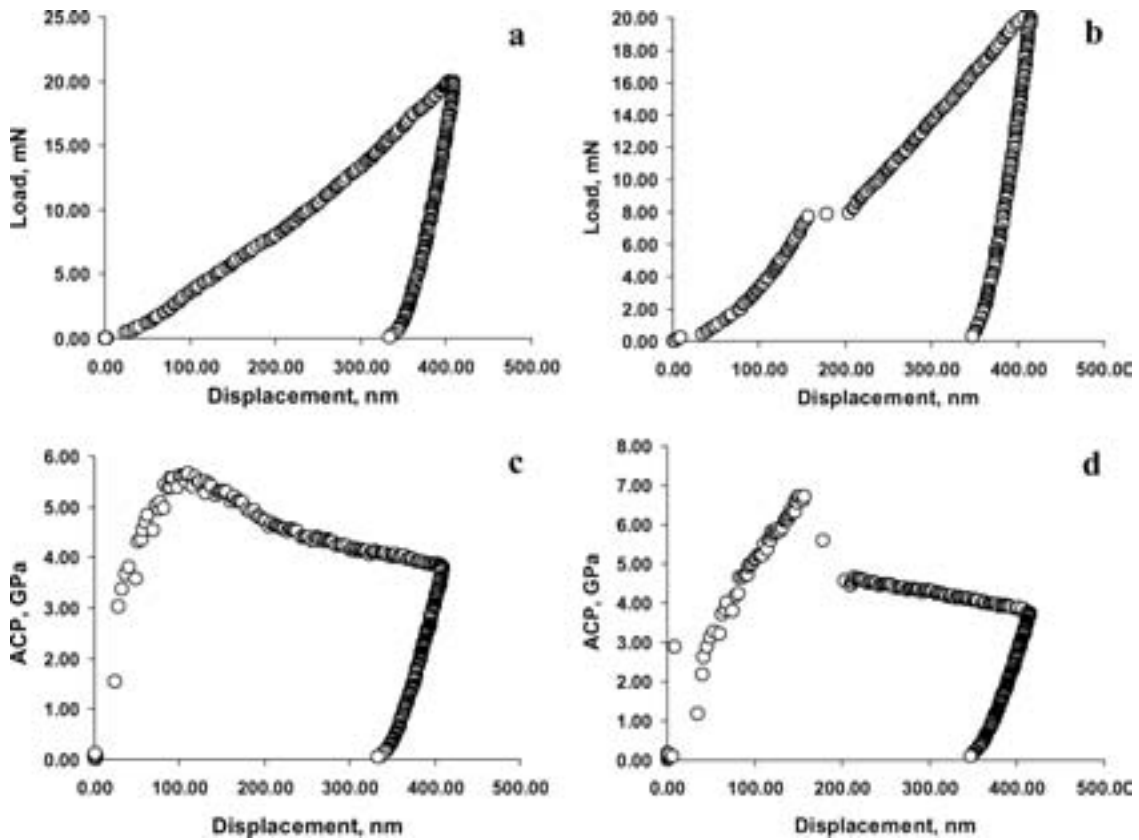


Figure 4 Load vs. displacement (a—without “pop-in”, b—with “pop-in”) and ACP vs. displacement (c—without “pop-in”, d—with “pop-in”) diagrams at a preset maximum displacement of 400 nm.

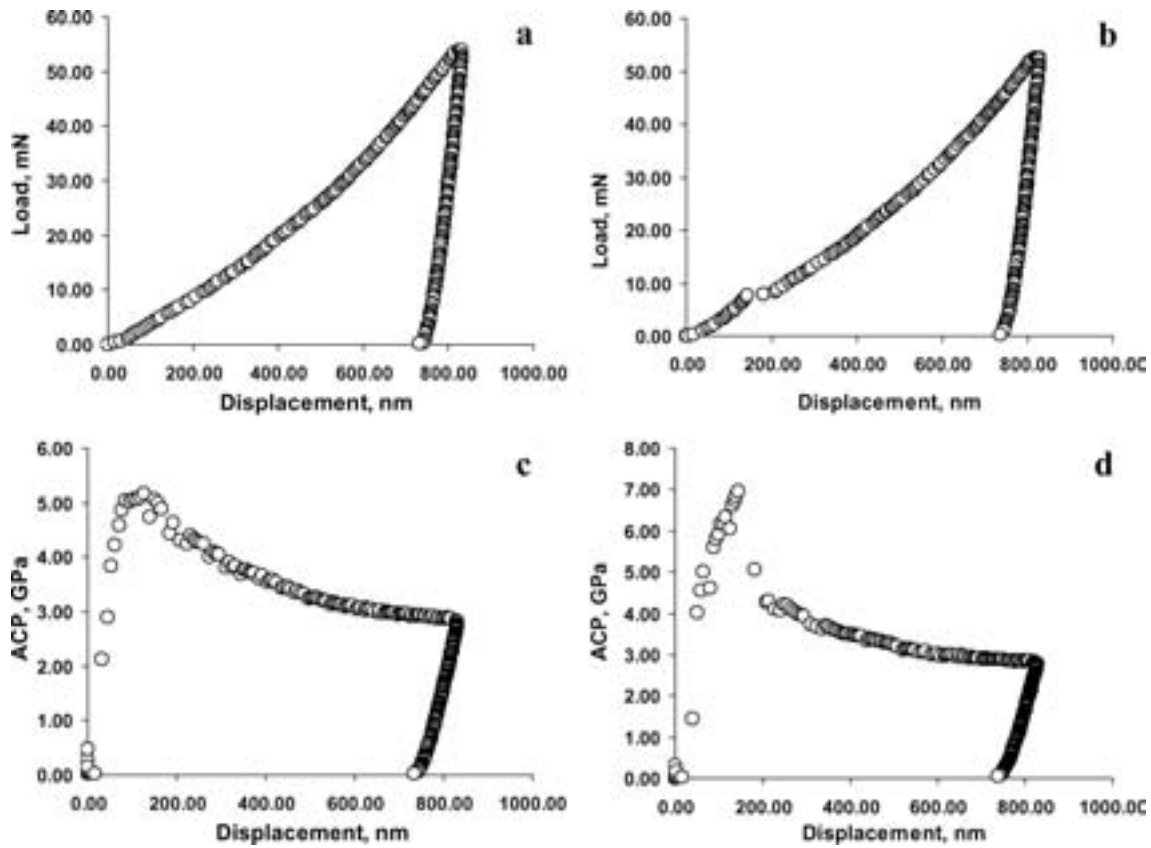


Figure 5 Load vs. displacement (a—without “pop-in”, b—with “pop-in”) and ACP vs. displacement (c—without “pop-in”, d—with “pop-in”) diagrams at a preset maximum displacement of 800 nm.

tically measured. As it was measured with a 50 nm displacement the hardness of the film was higher than that of the substrate, and the Young’s modulus of the film was lower than that of the substrate material. As the penetration depth increases, hardness decreases and Young’s modulus values increase from a value corresponding to the film material to a value corresponding to the substrate material (Fig. 6b). At an 800 nm displacement a measured hardness and Young’s modulus value approaches that of the substrate (Fig. 6a). At the same time, at a 50-nm displacement, a reduced hardness value is revealed, which can be associated with a substantial influence of the indenter tip shape at such shallow depths.

Superposition of ACP/displacement diagrams for preset displacements of 50, 200, 400, and 800 nm revealed that all the diagrams without “pop-in” are in a close agreement as if corresponding to a single diagram. The diagrams with “pop-in” are also practically coincident with a single diagram, except for the range of maximum ACP. In this range (at displacements of an order of 100 nm), when “pop-in” is observed, certain additional strengthening takes place (as compared to the cases without “pop-in”). In the case without “pop-in” the maximum ACP value is about 6.0 GPa, and in the case with “pop-in” this value is within 6.8–8.0 GPa. After reaching a maximum in the case with “pop-in” the pressure falls sharply with the penetration of an indenter in depth, and at a displacement

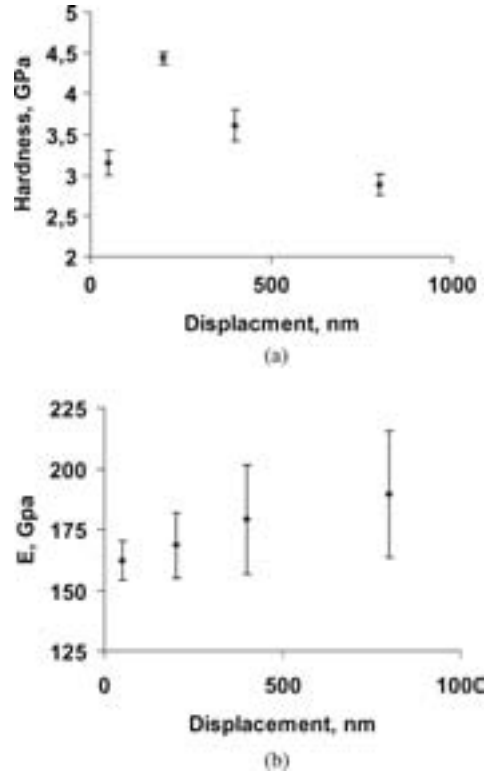


Figure 6 Hardness (a) and Young’s modulus (b) vs displacement diagrams for a  $\text{LaCrO}_3$  thin film.

of about 200 nm, it reaches the level corresponding to a single diagram.

Such “pop-ins” can be explained either by microcracking (fracture under the indenter) [30] or by an abrupt and irreversible phase transformation. It is known that  $\text{LaCrO}_3$  undergoes an orthorhombic to rhombohedral phase transition at pressures in the range of 1.1 to 5.4 GPa. During this phase a significant volume compression is observed which is principally due to discrete shrinkage of  $[\text{CrO}_6]$  octahedron. However, the pressure observed here for “pop-in” events is much higher and these events do not occur for all points tested in this study. Therefore the origin of the “pop-in” events is not completely understood.

#### 4. Summary

The deformation behavior of  $\text{LaCrO}_3$  under concentrated loads was investigated. The nanoindentation results were obtained for RF magnetron-sputtered  $\text{LaCrO}_3$  perovskite films deposited onto stainless steel substrates. Nanoindentation resulted in the two types of load–displacement diagrams. The majority of the diagrams refer to the first type, without any noticeable discontinuities. The second type of these diagrams is characterized by the presence of “pop-in”. To assess an elastic recovery level, residual displacement/maximum displacement as well as plastic strain work/total work of loading ratios were analyzed. At a given displacement, the  $h_f/h_{\max}$  ratios in the cases with “pop-in” and without it are practically coincident. The same relation is also valid for the  $W_p/W_t$  parameters, which is indicative of a weak influence of “pop-in”-associated processes on the elastic recovery and plasticity of the films.

ACP — displacement diagrams were calculated. The additional strengthening ahead of “pop-in” events (in comparison with the case without “pop-in”) was revealed. The nature of a “pop-ins” and strengthening effects remains uncertain and requires further investigations.

#### Acknowledgments

The work at Drexel University was supported by the National Science Foundation through Grant number DMR-0201770 and National Energy Technology Laboratory, US Department of Energy under Contract # 239811

#### References

1. W. OLIVER and G. PHARR, *J. Mater. Res.* **7** (1992) 1564.
2. A. GOULDSTONE, H.-J. KOH, K.-Y. ZENG, A. E. GIANNAKOPOULOS and S. SURESH, *Acta Mater.* **48** (2000) 2277.
3. J. L. HAY and G. PHARR, in *Mechanical Testing and Evaluation*, edited by H. KUHN and D. MEDLIN (ASM International, Materials Park, OH, 2000) p. 231.

4. N. ORLOVSKAYA, Y. GOGOTSI, M. REECE, B. CHENG and I. GIBSON, *Acta Mater.* **50** (2002) 715.
5. Y. GAILLARD, C. TROMAS and J. WOIRGARD, *Acta Mater.* **51** (2003) 1059.
6. T. JULIANO, Y. GOGOTSI and V. DOMNICH, *J. Mater. Res.* **18** (2003) 1192.
7. N. ORLOVSKAYA, C. JOHNSON and R. GEMMEN, unpublished results.
8. C. P. KHATTAK and D. E. COX, *Mater. Res. Bull.* **12** (1977) 463.
9. T. HASHIMOTO, N. MATSYSHITA, Y. MURAKAMI, N. KOJIMA, K. YOSHIDA, H. TAGAWA, M. DOKIYA and T. KIKEGAWA, *Solid State Comm.* **108** (1998) 691.
10. T. HASHIMOTO, N. TSUZUKI, A. KISHI, K. TAKAGI, K. TSUDA, M. TANAKA, K. OIKAWA, T. KAMIYAMA, K. YOSHIDA, H. TAGAWA and M. DOKIYA, *Solid State Ionics* **132** (2000) 183.
11. K. OIKAWA, T. KAMIYAMA, T. HASHIMOTO, Y. SHIMOJOYO and Y. MORII, *J. Solid State Chem.* **154** (2000) 524.
12. H. HAYASHI, M. WATANABE and H. INABA, *Thermochi. Acta* **359** (2000) 77.
13. R. A. SWALIN, in “Thermodynamics of Solids”. (John Wiley & Sons, Inc., New York, 1962).
14. W. Z. ZHU and S. C. DEEVI, *Mat Sci. Eng.* **A348** (2003) 227.
15. C. JOHNSON, R. GEMMEN and N. ORLOVSKAYA, *Composites, Part B: Engineering* **35** (2004) 167.
16. D. B. MEADOWCROFT, P. G. MEIER and A. C. WARREN, *Energy Convers.* **12** (1972) 145.
17. I. YASUDA and M. HISHINUMA, *J. Solid State Chem.* **115** (1995) 152.
18. A. VASINONTA and J. L. BEUTH, *Eng. Fract. Mech.* **68** (2001) 843.
19. N. ORLOVSKAYA, A. CORATOLO, C. JOHNSON and R. GEMMEN, *J. Am. Ceram. Soc.* (2004), accepted.
20. M. MARTIN and M. TROYON, *J. Mater. Res.* **17** (2002) 2227.
21. N. V. NOVIKOV, S. N. DUB, YU. V. MILMAN, I. V. GRIDNEVA and S. I. CHUGUNOVA, *J. Superhard Mater.* **18** (1996) 32.
22. S. DUB, N. NOVIKOV and Y. MILMAN, *Phil. Mag.* **A82** (2002) 2161.
23. E. R. WEPPELMAN, J. S. FIELD and M. V. SWAIN, *J. Mater. Res.* **8** (1993) 830.
24. A. BOLSHAKOV and G. M. PHARR, *ibid.* **13** (1998) 1049.
25. M. SAKAI, *ibid.* **14** (1999) 3630.
26. A. E. GIANNAKOPOULOS and S. SURESH, *Scripta Mat.* **40** (1999) 1191.
27. M. DAO, N. CHOLLACOOP, K. J. VAN VLIET, T. A. VENKATESH and S. SURESH, *Acta Mat.* **49** (2001) 3899.
28. T. F. PAGE and S. V. HAINSWORTH, *Surf. Coat. Technol.* **61** (1993) 201.
29. W. LEE KITTY, Y.-W. CHUNG, C. Y. CHAN, I. BELLO, S. T. LEE, A. KARIMI, J. PATSCHEIDER, M. P. DELPLANCKE-OGLETREE, D. YANG, B. BOYCE and T. BUCHHEIT, *ibid.* **168** (2003) 57.
30. D. F. BAHR, M. PANG and D. RODRIGUEZ-MAREK, in *MRS Symposium Proceedings, Fundamentals of Nanoindentation and Nanotribology II*, edited by S. P. Baker, R. F. Cook, S. G. Corcoran and N. R. Moody (MRS, Pittsburgh, 2001) Vol. 649, p. Q4.2.

Received 27 July 2004

and accepted 20 April 2005